International Journal of Nanomedicine

Dovepress

open access to scientific and medical research

Open Access Full Text Article

ORIGINAL RESEARCH

Size-dependent cytotoxicity of Fe_3O_4 nanoparticles induced by biphasic regulation of oxidative stress in different human hepatoma cells

This article was published in the following Dove Press journal:
International Journal of Nanomedicine
29 July 2016
Number of times this article has been viewed

Yuexia Xie[1,2,*]
Dejun Liu[3,*]
Chenlei Cai[1,*]
Xiaojing Chen[1]
Yan Zhou[1]
Liangliang Wu[1]
Yongwei Sun[3]
Huili Dai[1,2]
Xianming Kong[1,2]
Peifeng Liu[1,2]

[1]Central Laboratory, [2]State Key Laboratory of Oncogenes and Related Genes, Shanghai Cancer Institute, [3]Department of Biliary-Pancreatic Surgery, Renji Hospital, School of Medicine, Shanghai Jiao Tong University, Shanghai, People's Republic of China

*These authors contributed equally to this work

Correspondence: Huili Dai; Peifeng Liu
State Key Laboratory of Oncogenes and Related Genes, Shanghai Cancer Institute, Renji Hospital, School of Medicine, Shanghai Jiao Tong University, No 25/Ln 2200 Xietu Road, Shanghai 200032, People's Republic of China
Email dhl_sh@163.com; liupeifeng@yahoo.com

Abstract: The application of Fe_3O_4 nanoparticles (NPs) has made great progress in the diagnosis of disease and in the drug delivery system for cancer therapy, but the relative mechanisms of potential toxicity induced by Fe_3O_4 have not kept pace with its development in the application, which has hampered its further clinical application. In this article, we used two kinds of human hepatoma cell lines, SK-Hep-1 and Hep3B, to investigate the cytotoxic effects and the involved mechanisms of small Fe_3O_4 NPs with different diameters (6 nm, 9 nm, and 14 nm). Results showed that the size of NPs effectively influences the cytotoxicity of hepatoma cells: 6 nm Fe_3O_4 NPs exhibited negligible cytotoxicity and 9 nm Fe_3O_4 NPs affected cytotoxicity via cellular mitochondrial dysfunction and by inducing necrosis mediated through the mitochondria-dependent intracellular reactive oxygen species generation. Meanwhile, 14 nm Fe_3O_4 NPs induced cytotoxicity by impairing the integrity of plasma membrane and promoting massive lactate dehydrogenase leakage. These results explain the detailed mechanism of different diameters of small Fe_3O_4 NPs-induced cytotoxicity. We anticipate that this study will provide different insights into the cytotoxicity mechanism of Fe_3O_4 NPs, so as to make them safer to use in clinical application.

Keywords: hepatoma cells, nanoparticles, cytotoxicity, mechanism, oxidative stress

Introduction

Magnetic iron oxide (Fe_3O_4) nanoparticles (NPs) have been applied in a wide range of biomedical and medical areas, including cell labeling,[1,2] separation and tracking,[3] drug delivery,[4] diagnosis,[5] and hyperthermia for cancer therapy.[6] Due to the unique properties of Fe_3O_4 NPs, much progress in the development of its application has been made. However, further research is required in understanding the interaction of Fe_3O_4 NPs within biological systems. As Fe_3O_4 NPs more easily enter cells than traditional chemical reagents,[7] their toxicity is a potential risk inevitably existing in the medical application.

Toxicological response of Fe_3O_4 NPs differs according to their diameter, charge, dose, structures, and surface properties.[8] The oxidative stress induced by the elevation of intracellular reactive oxygen species (ROS) generation and lipid peroxidation and the depletion of superoxide dismutase (SOD), glutathione, and catalase (CAT) activities are proved to be the principal reasons that cause toxicological response.[9] Moreover, toxicological response of NPs varied with the change of cell types, suggesting the complexity of toxicological response of NPs.[10] Notably, however, most of the toxicity research mainly focuses on the NPs with ≥20 nm diameter; the toxicological effect of small particles (≤20 nm) is poorly understood and the mechanisms of

submit your manuscript | www.dovepress.com
Dovepress
http://dx.doi.org/10.2147/IJN.S105575

toxicological hazards have not been fully evaluated; small particles are believed to interact more strongly with biological systems, through either enhanced cellular uptake or faster decomposition due to greater surface area-to-volume ratios, compared to larger particles.[11] It is therefore necessary to investigate the toxicity and relative mechanism of small Fe_3O_4 NPs in different cells so as to understand and mitigate any possible toxicity response that may be associated with exposure.

After intravenous injection, the in vivo distribution of nontargeted NPs mainly depends on their diameter. NPs with ≥200 nm diameter are generally found in the reticuloendothelial system, while NPs <200 nm can be enriched in the solid tumor.[12] Ten-nanometer NPs showed the highest cytotoxicity of hepatoma cells compared to 50 nm and 100 nm.[13] The liver is one of the primary sites of uptake after intravenous administration, and hepatic cells are continuously exposed to the NPs, so that administered NPs accumulate at higher level in the liver than in other tissues. Nowadays, NPs-based drug delivery system is a prospective therapeutic strategy and suited for the treatment of liver disease,[14] including hepatocellular carcinoma,[14] liver fibrosis,[15,16] and viral hepatitis.[17] Therefore, we chose to analyze the toxicity of small Fe_3O_4 NPs using hepatoma cells. Specifically, in this study, the small Fe_3O_4 NPs with different diameters (6 nm, 9 nm, and 14 nm) were investigated in two kinds of hepatoma cells (SK-Hep-1 and Hep3B), which contributed to the understanding of the relative mechanism of toxicological response difference in different cells, so as to realize their toxicity hazard and further promote their security application.

Materials and methods

Materials

$Fe(acac)_3$ was purchased from Acros (Pittsburgh, PA, USA). Triethylene glycol was purchased from Sigma-Aldrich (St Louis, MO, USA). Fetal bovine serum (FBS), Dulbecco's Modified Eagle's Medium (DMEM), minimum essential medium, penicillin, streptomycin, and 0.25% ethylenediaminetetraacetic acid trypsin were purchased from Thermo Fisher Scientific (Waltham, MA, USA). SOD, CAT, 2′,7′-dichlorofluorescein diacetate (DCFH-DA), phenylmethanesulfonyl fluoride, and lactate dehydrogenase (LDH) Cytotoxicity Assay Kit were purchased from Beyotime Institute of Biotechnology (Nantong, People's Republic of China). Cell Counting Kit-8 (CCK-8) was purchased from Dojindo (Kumamoto, Japan). Annexin V-FITC/Dead Cell Apoptosis Kit was purchased from Molecular Probes (Eugene, OR, USA). Antibodies including Akt, p-Akt (Ser473), Erk1/2, p-Erk1/2 (Thr202/Tyr204), p38, and p-p38 (Thr180/Tyr182) were purchased from Cell Signaling Technology (Danvers, MA, USA). β-actin antibody was obtained from HuaAn Biotechnology (Hangzhou, People's Republic of China). IRDye 800CW conjugated secondary antibody was obtained from LI-COR Biosciences (Lincoln, NE, USA). M-PER Mammalian Protein Extraction Reagent and bicinchoninic acid (BCA) Protein Assay Kit were purchased from Thermo Fisher Scientific. Complete inhibitor cocktail was purchased from Hoffman-La Roche Ltd. (Basel, Switzerland). Nitrocellulose membrane was purchased from Whatman (Maidstone, UK).

Hepatoma cell lines, SK-Hep-1 and Hep3B, were obtained from the Shanghai Cell Bank of China (Shanghai, People's Republic of China). SK-Hep-1 cells were maintained in DMEM containing 4.5 g/L glucose. Hep3B cells were grown in minimum essential medium. Both culture media contained 100 U/mL penicillin, 100 μg/mL streptomycin, and 10% FBS. All cultures were maintained at 37°C in a fully humidified incubator with 5% CO_2. The study protocols were approved by the Hospital Research Ethics Committees of Renji Hospital. All methods were carried out in accordance with the approved guidelines.

Nanomaterials synthesis and characterization

Six-nanometer Fe_3O_4 NPs were prepared using the polyol method.[18] Then, 2 mmol of $Fe(acac)_3$ and 25 mL of triethylene glycol were directly added into a three-neck round-bottomed flask equipped with condenser, magnetic stirrer, thermograph, and heating mantle, and stirred under argon. The mixture was heated to 180°C at a rate of 3°C/min and kept at that temperature for 30 minutes, then quickly heated to reflux (280°C) and kept at reflux for another 28 minutes. After cooling down to room temperature, a black homogeneous colloidal suspension containing magnetite NPs was obtained. The homogeneous colloidal suspension was dialyzed in distilled water and then collected using a magnetic separation method to obtain 6 nm Fe_3O_4 NPs.

Using seed-mediated growth method, 9 nm and 11 nm Fe_3O_4 NPs were synthesized. Briefly, 2 mmoL $Fe(acac)_3$ was added to the synthetic 6 nm Fe_3O_4 NPs solution to react according to the reaction condition of 6 nm Fe_3O_4 NPs. Subsequently, the obtained solution was dialysis in distilled water and then collected with a magnetic to obtain 9 nm Fe_3O_4 magnetic nanoparticles. Similarly, 2 mmoL $Fe(acac)_3$ was added to 9 nm Fe_3O_4 NPs solution to react according to the reaction condition of 6 nm Fe_3O_4 NPs. The obtained solution was then dialysis in distilled water and collected with a magnetic to obtain 14 nm Fe_3O_4 magnetic nanoparticles.

The size of the Fe_3O_4 NPs was measured using an HT7700 transmission electron microscope (TEM; Hitachi Ltd., Tokyo, Japan) operated at an acceleration voltage of 200 kV, and the size distribution of the Fe_3O_4 NPs was determined using a Zetasizer Nano-Zsp analyzer (Malvern Instruments, Malvern, UK).

Quantitative measurement of cellular uptake of NPs

The flow cytometry was used to measure the cellular contents after treatment with Fe_3O_4 NPs. SK-Hep-1 and Hep3B cells (5×10^5 cells/well) were separately seeded into six-well plates and incubated for 24 hours, and then exposed to Fe_3O_4 NPs for another 24 hours. Cells were washed with cold phosphate-buffered saline (PBS) and harvested by trypsinization. Then, the collected cells were suspended with PBS at the concentration of 1×10^6 cells/mL, and the cellular uptake amount was quantitatively determined by BD FACSCalibur flow cytometry (BD Biosciences, San Jose, CA, USA).

Internalization and localization of Fe_3O_4 NPs

Internalization and localization of Fe_3O_4 NPs in cells were observed using TEM.[19] SK-Hep-1 cells (6×10^6 cells/well) were seeded in 10 cm plates and incubated for 24 hours, and then exposed to Fe_3O_4 NPs for another 24 hours. Cells were washed three times with PBS, trypsinized, harvested, and resuspended in 500 µL of stationary liquid containing 4% paraformaldehyde and 5% glutaraldehyde. Cells were embedded in agar gel, which was then cut into 1 mm slices. Each slice was again fixed using osmic acid and dehydrated, embedded, and imaged using TEM.

Mitochondrial function

Mitochondrial function was detected using CCK-8 on a microplate reader (BioTek, Winooski, VT, USA). SK-Hep-1 and Hep3B cells (2×10^4 cells/well) were separately seeded in 96-well plates and incubated for 24 hours, and then exposed to Fe_3O_4 NPs for another 24 hours. Then, 10 µL of CCK-8 reagent was added and incubated for 1 hour at 37°C. Finally, the absorbance was measured at 450 nm. The untreated cells served as the control, and their mitochondrial function was defined as 100%.

ROS assay

Intracellular ROS levels were detected using DCFH-DA and analyzed by FACSCalibur flow cytometer. SK-Hep-1 and Hep3B cells (5×10^5 cells/well) were separately seeded into six-well plates and incubated for 24 hours, and then exposed to Fe_3O_4 NPs for another 24 hours. Cells were washed with FBS free medium and incubated with 10 µM DCFH-DA for 30 minutes at 37°C in the dark. Subsequently, cells were washed twice with FBS free medium to remove the additional dye, and incubated in FBS free medium for an additional 30 minutes at 37°C to allow complete de-esterification of the intracellular diacetates. Finally, cells were harvested by trypsinization, and at least 2×10^4 cells from each sample were analyzed by FACSCalibur flow cytometer.

Apoptosis and necrosis assays

Apoptosis and necrosis were detected using Annexin V-FITC/Dead Cell Apoptosis Kit and analyzed by FACSCalibur flow cytometer. SK-Hep-1 and Hep3B cells (5×10^5 cells/well) were separately seeded into six-well plates and incubated for 24 hours, and then exposed to Fe_3O_4 NPs or Fe_3O_4 NPs combined with 500 U/mL SOD plus 500 U/mL CAT for 24 hours. Cells were washed with cold PBS, harvested by trypsinization, and resuspended in 100 µL 1× annexin-binding buffer containing 5 µL annexin V and 1 µL of 100 µg/mL propidium iodide (PI) for 15 minutes at room temperature in the dark. After the incubation period, 400 µL 1× annexin-binding buffer was added to each sample and mixed gently. At least 2×10^4 cells from each sample were analyzed. Annexin V^+ staining indicated cells in the process of apoptosis due to the potent affinity of annexin V for phosphatidylserine, which transports annexin V protein from the inner leaflet of the plasma membrane to the outer surface of the membrane. Meanwhile, annexin V^-/PI^+ staining marked necrotic cells, since PI could penetrate the compromised membranes of cells that are dead instead of the intact cell membranes of viable cells.

Western blot assays

After treating with Fe_3O_4 NPs for 24 hours, cells (2×10^6 cells in 60 mm dish) were washed three times with cold PBS and lysed using M-PER Mammalian Protein Extraction Reagent supplemented with complete inhibitor cocktail and phenylmethanesulfonyl fluoride. The protein concentration in the supernatant fraction was determined by the pierce BCA Protein Assay Kit. Equal amounts of protein were separated by 10%–12% sodium dodecyl sulfate-polyacrylamide gel electrophoresis and transferred onto a nitrocellulose membrane. After blocking with 5% ChromatoPur bovine serum albumin in Tris-buffered saline for 1 hour, the membrane was incubated with the primary antibody at 4°C overnight as indicated. Then, the membrane was washed with Tris-buffered saline Tween-20 and incubated with secondary antibodies at room temperature for 1 hour. After several

washes, protein bands were visualized using an Odyssey infrared imaging system (LI-COR Biosciences) and quantified with Odyssey application software. β-actin was used for the loading control.

Cellular membrane damage assay

The cellular membrane damage assay was performed using the LDH Cytotoxicity Assay Kit that can quantitatively evaluate the degree of cellular membrane damage associated with the leakage of the cytosolic LDH. SK-Hep-1 and Hep3B cells (2×10^4 cells/well) were separately seeded in 96-well plates and incubated for 24 hours. The media were replaced with Fe_3O_4 NPs or Fe_3O_4 NPs plus chemicals in 150 μL for another 24 hours. One hour before harvesting the supernatants, 15 μL of the lysis solution was added to the wells containing the target cell maximum LDH release control. Then, the plate was centrifuged at 400× *g* for 5 minutes and 120 μL supernatant from each well was transferred to a new 96-well plate. Subsequently, 60 μL of the substrate mix was added and incubated for 15 minutes at room temperature. Finally, the absorbance was measured on a microplate reader (BioTek) at 490 nm. Cytotoxicity was calculated as follows:

$$\text{Cytotoxicity}(\%) = \frac{\text{Experimental} - \text{Target spontaneous}}{\text{Target maximum} - \text{Target spontaneous}} \times 100\%$$

Statistical analysis

The data were expressed as mean ± standard error of at least three independent experiments. The significance of differences in the data of different groups was appropriately determined by the unpaired Student's *t*-test at $P<0.05$.

Results

Characterization of Fe_3O_4 NPs

In order to investigate the relative mechanism of size-dependent cytotoxicity of Fe_3O_4 NPs for different hepatoma cells, we successfully synthesized the Fe_3O_4 NPs with sizes of 6 nm, 9 nm, and 14 nm. TEM results verified that 6 nm, 9 nm, and 14 nm Fe_3O_4 NPs were well dispersed in size and spherical in shape (Figure 1A–D), and they had uniform size distribution and similar zeta potential from –20 mV to –30 mV (Figure 1E), which was beneficial to subsequently evaluate the influence of particles size for hepatoma cells.

Cellular uptake of Fe_3O_4 NPs

Figure 2A and B show the flow cytometric light scatter histograms of SK-Hep-1 cells treated with 200 μg/mL or 500 μg/mL Fe_3O_4 NPs with different diameters (6 nm, 9 nm, and 14 nm) for 24 hours. The side-scattered intensity (reflecting cellular uptake) of SK-Hep-1 cells increased in a dose-dependent manner, that is, the cells that took up higher doses of Fe_3O_4 NPs showed higher side scatter. However, in this case, the intracellular accumulation of Fe_3O_4 NPs with 9 nm diameters is much higher than that with 6 nm or 14 nm diameters, and the uptake efficiency of Fe_3O_4 NPs with 14 nm diameters is also much higher than that with 6 nm diameters. Interestingly, similar results were obtained in Hep3B cells (Figure 2C and D). These experiments demonstrate that the size of particles effectively influences the cellular uptake of Fe_3O_4 NPs, with the cellular uptake of 9 nm >14 nm >6 nm.

Internalized distribution of Fe_3O_4 NPs

We subsequently detected the internalized distribution of Fe_3O_4 NPs in hepatoma cells through TEM, using the SK-Hep-1 cells as model cells. As illustrated in the TEM images (Figure 3), the internalization distribution of Fe_3O_4 NPs inside the SK-Hep-1 cells is closely related to their size and concentration. More Fe_3O_4 NPs were internalized in the cellular cytoplasm when incubating the cells at higher dosage. These data also further demonstrate the findings of flow cytometry; the uptake quantity of Fe_3O_4 NPs was mainly influenced by the size of the particles.

Effect of Fe_3O_4 NPs on cellular mitochondrial function

Mitochondria are vulnerable targets for toxic injury due to their important role in maintaining cellular function. In this experiment, the size-dependent concurrent effect of Fe_3O_4 NPs on the cellular mitochondrial function was investigated. As shown in Figure 4A, the mitochondrial function of SK-Hep-1 cells exposed to 6 nm Fe_3O_4 NPs for 24 hours was slightly decreased only at higher doses than 400 μg/mL. Similarly, when exposed to 14 nm Fe_3O_4 NPs, the mitochondrial function was gradually decreased in a dose-dependent manner and such inhibition was statistically significant over 200 μg/mL. However, 9 nm Fe_3O_4 NPs exhibited significant effects on the mitochondrial function in a dose-dependent manner in sharp contrast with the 6 nm and 14 nm Fe_3O_4 NPs, in which 14 nm Fe_3O_4 NPs exhibited more toxicity than 6 nm Fe_3O_4 NPs (Figure 4A). Similarly, 6 nm, 9 nm, and 14 nm Fe_3O_4 NPs generated similar tendency of mitochondrial function inhibition in Hep3B cells (Figure 4B). The data together with the cellular internalized ability suggest that the intracellular accumulation of Fe_3O_4 NPs is involved in the cellular mitochondrial dysfunction.

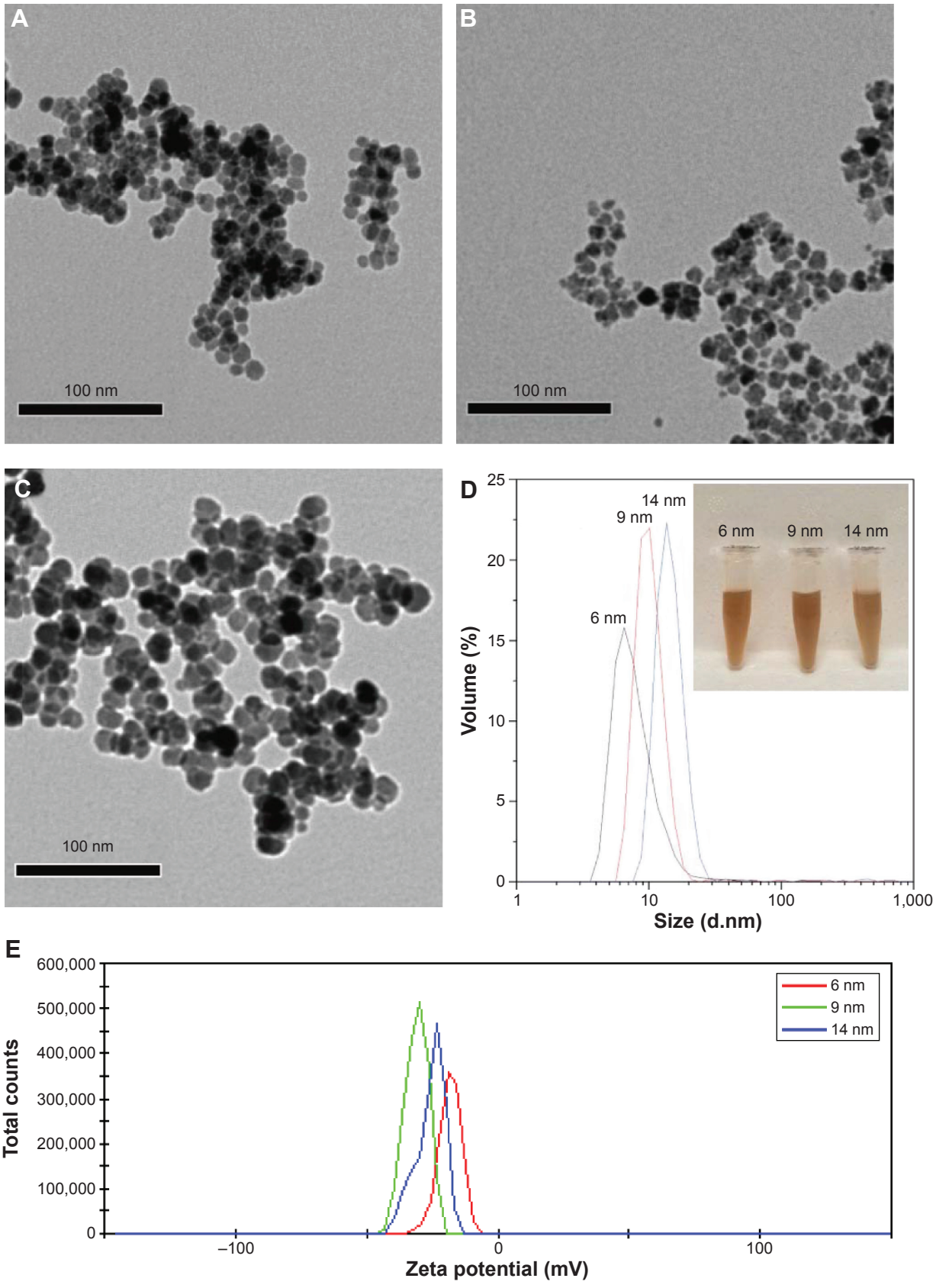

Figure 1 Characterization of Fe_3O_4 NPs.
Notes: TEM images of Fe_3O_4 NPs with the diameter of 6 nm (**A**), 9 nm (**B**), and 14 nm (**C**). (**D**) The size distribution images of Fe_3O_4 NPs; the inserted image is the image of Fe_3O_4 NPs aqueous solution. (**E**) The zeta potential image of Fe_3O_4 NPs.
Abbreviations: NPs, nanoparticles; TEM, transmission electron microscope.

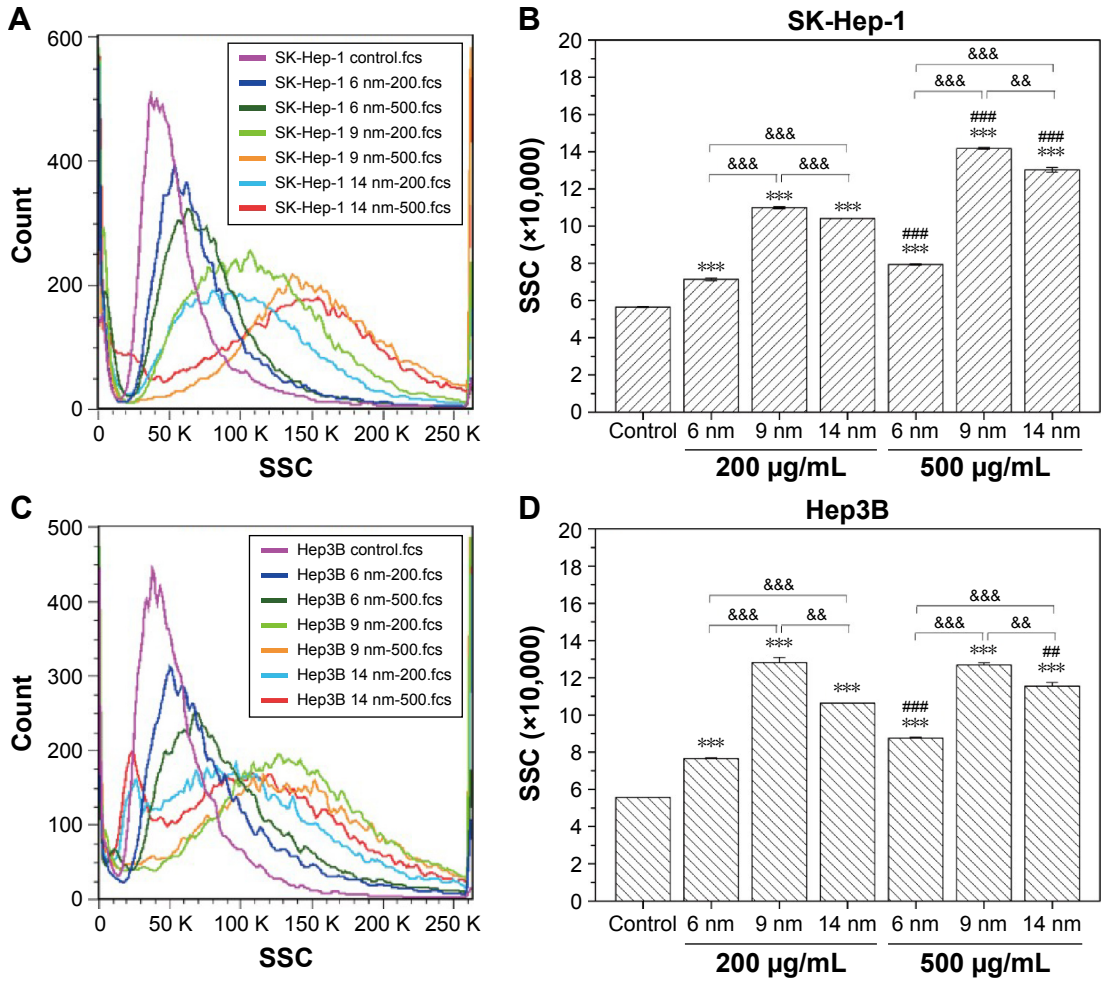

Figure 2 Cellular uptake of Fe_3O_4 NPs with different diameter sizes in human hepatoma SK-Hep-1 cells (**A** and **B**) and Hep3B cells (**C** and **D**) after exposure for 24 hours. Fe_3O_4 NPs-treated cells were determined by flow cytometry.

Notes: Cells incubated in medium only were used as control. Results correspond to mean ± SE of three independent experiments with triplicates in each case. $^{***}P<0.001$ compared to the control without Fe_3O_4 NPs treatment; $^{\#\#}P<0.01$, $^{\#\#\#}P<0.001$ compared to the corresponding Fe_3O_4 NPs treatment at 200 μg/mL; $^{\&\&}P<0.01$, $^{\&\&\&}P<0.001$ between the indicated groups.

Abbreviations: fcs, flow cytometers; NPs, nanoparticles; SE, standard error; SSC, side scatter.

Generation of Fe_3O_4 NPs-induced ROS

To further illustrate the mechanism of mitochondrial dysfunction induced by Fe_3O_4 NPs, the ability of Fe_3O_4 NPs to induce oxidative stress was evaluated by detecting the levels of intracellular ROS. A significant increase in ROS was observed after 24 hours exposure of SK-Hep-1 and Hep3B cells to Fe_3O_4 NPs (Figure 5). The ROS level in SK-Hep-1 cells was increased in a dose-dependent manner after treating with the same kind of Fe_3O_4 NPs. However, at both 200 μg/mL and 500 μg/mL, 9 nm Fe_3O_4 NPs induced the highest level of ROS compared to the other particles; a sign of overwhelming oxidative stress. Meanwhile, the ROS activity was found to be remarkably stronger for 14 nm Fe_3O_4 NPs than for 6 nm Fe_3O_4 NPs. Similar findings were also observed in Hep3B cells. These results demonstrate that ROS play a leading role in mitochondrial dysfunction, especially for 9 nm Fe_3O_4 NPs treatment.

Cell necrosis in Fe_3O_4 NPs-treated cells

We further investigated the apoptotic and necrotic effect induced by Fe_3O_4 NPs using annexin V/PI double-staining method. Figure 6 shows the indexes of apoptotic and necrotic cells for SK-Hep-1 (Figure 6A) and Hep3B cells (Figure 6B) after 24 hours of exposure to 200 μg/mL and 500 μg/mL Fe_3O_4 NPs with 6 nm, 9 nm, and 14 nm particle sizes. Interestingly, the levels of apoptosis for SK-Hep-1 and Hep3B cells treated with different Fe_3O_4 NPs were observed to be similar to those in the control group. Then, 6 nm and 14 nm Fe_3O_4 NPs at a dose of 500 μg/mL triggered a slight increased amount of necrotic cells, while 9 nm Fe_3O_4 NPs treatment resulted in a significant increased amount of necrotic cells, which was associated with the concentration of 9 nm Fe_3O_4 NPs. These results indicate that, in contrast with 6 nm and 14 nm, 9 nm Fe_3O_4 NPs predominantly contributed to cell necrosis.

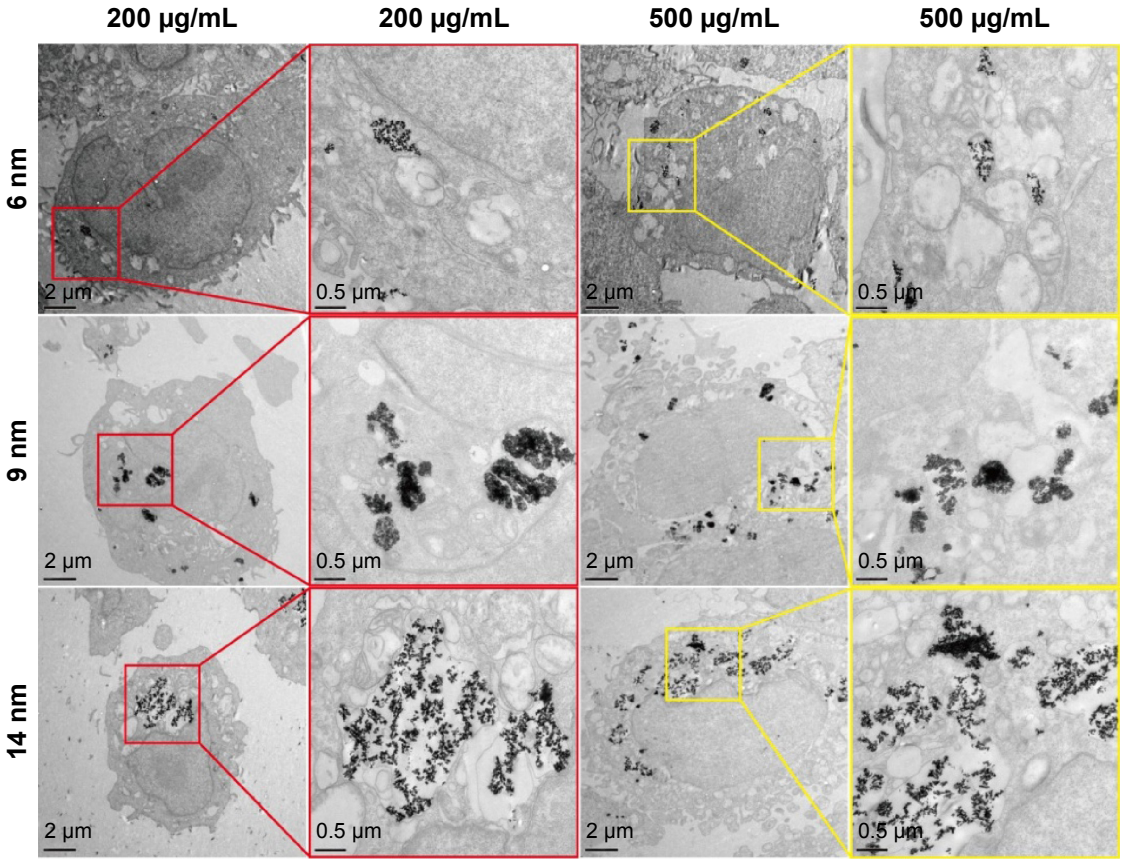

Figure 3 Internalization and localization of Fe_3O_4 NPs with different diameters in human hepatoma SK-Hep-1 cells after exposure for 24 hours.
Notes: Cells treated with Fe_3O_4 NPs were determined by TEM. Fe_3O_4 NPs are enclosed in vesicles.
Abbreviations: NPs, nanoparticles; TEM, transmission electron microscope.

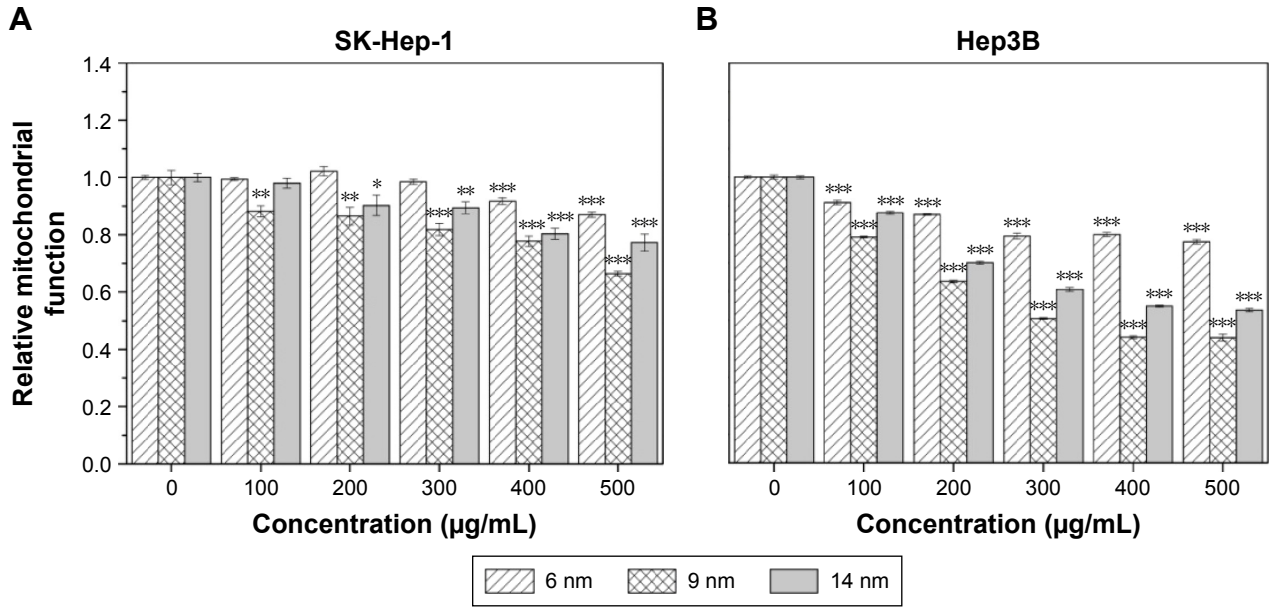

Figure 4 Effect of Fe_3O_4 NPs on mitochondrial function of human hepatoma SK-Hep-1 cells (**A**) and Hep3B cells (**B**).
Notes: Mitochondrial function of cells treated with various concentrations of Fe_3O_4 NPs with different diameters for 24 hours was measured by the CCK-8 assay. Data are presented as mean ± SE of three independent experiments with six replicates in each case. *$P<0.05$, **$P<0.01$, ***$P<0.001$ compared to the control without Fe_3O_4 NPs treatment.
Abbreviations: CCK-8, Cell Counting Kit-8; NPs, nanoparticles; SE, standard error.

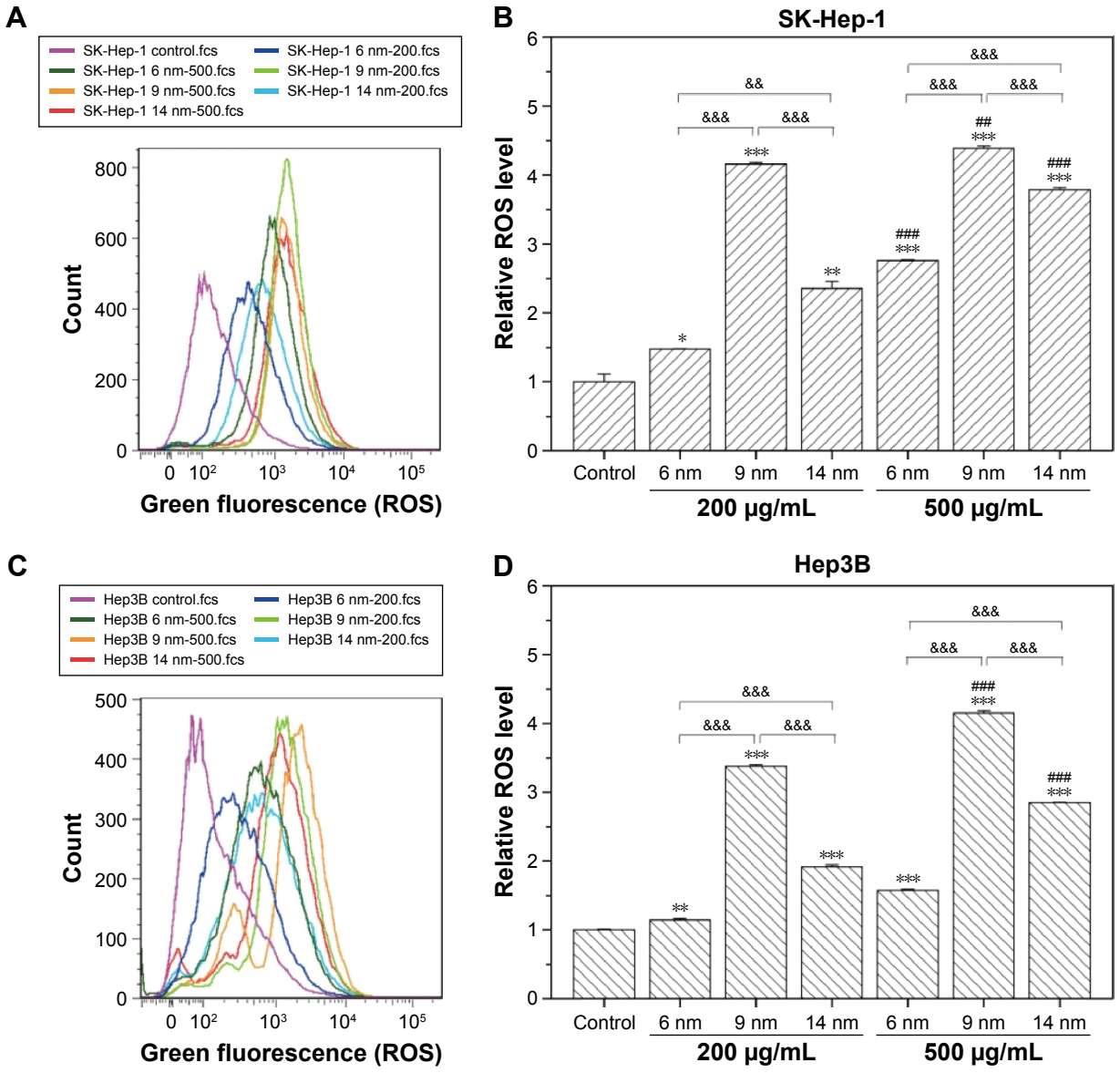

Figure 5 Influence of Fe_3O_4 NPs on the induction of ROS in human hepatoma SK-Hep-1 cells (**A** and **B**) and Hep3B cells (**C** and **D**).
Notes: Fe_3O_4 NPs-treated cells were determined by flow cytometry. Cells incubated in medium only were used as control. Results correspond to mean ± SE of three independent experiments. $^{*}P<0.05$, $^{**}P<0.01$, $^{***}P<0.001$ compared to the control without Fe_3O_4 NPs treatment; $^{\#\#}P<0.01$, $^{\#\#\#}P<0.001$ compared to the corresponding Fe_3O_4 NPs treatment at 200 μg/mL; $^{\&\&}P<0.01$, $^{\&\&\&}P<0.001$ between the indicated groups.
Abbreviations: fcs, flow cytometers; NPs, nanoparticles; ROS, reactive oxygen species; SE, standard error.

Influence of Fe_3O_4 NPs on Akt and MAPK/Erk signaling pathways in hepatoma cells

MAPK/Erk and Akt pathways are often involved in the regulation of cell survival, apoptosis, and necrosis. Therefore, we further detected the corresponding proteins and their activation situation. The results of Western blot assay (Figure 7) showed that the expression levels of p-Akt and p-Erk were significantly upregulated after Fe_3O_4 NPs treatment. The increases in p-Akt and p-Erk were more prominent in 9 nm Fe_3O_4 NPs treatment than 6 nm or 14 nm Fe_3O_4 NPs treatment at 200 μg/mL, and 9 nm and 14 nm Fe_3O_4 NPs triggered higher expression of p-Akt and p-Erk treatment than 6 nm at 500 μg/mL. In addition, p-p38, acted as proapoptotic and necrotic stimuli, dramatically increased in 9 nm Fe_3O_4 NPs-treated cells at both 200 μg/mL and 500 μg/mL, which was in good agreement with the results of annexin V/PI double staining, verifying that 9 nm Fe_3O_4 NPs greatly induced cellular necrosis.

ROS scavenger suppresses Fe_3O_4 NPs-induced necrosis and plasma membrane damage

To confirm the critical role of oxidative stress induced by Fe_3O_4 NPs in promoting cellular necrosis, we treated cells

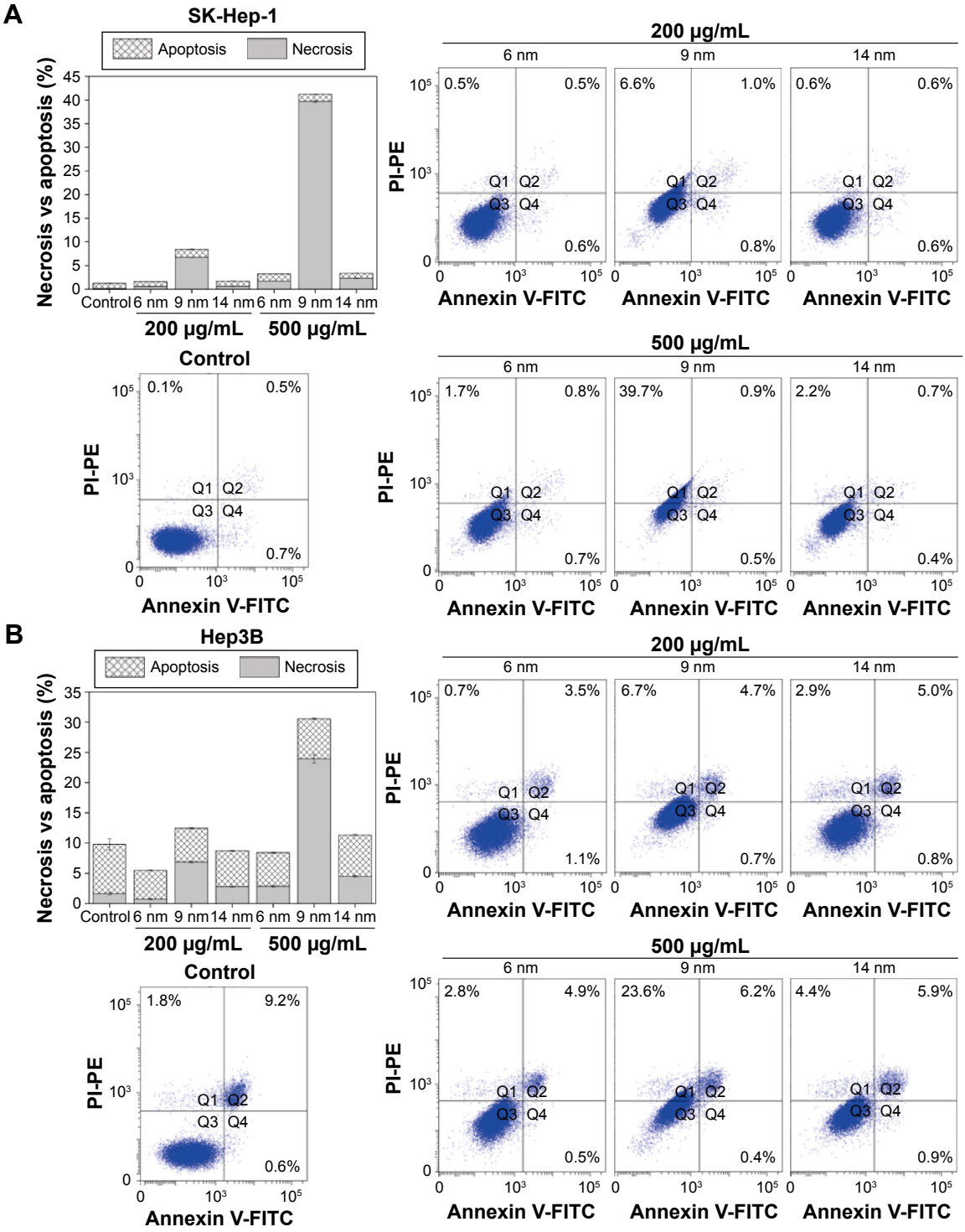

Figure 6 Induction of apoptosis and necrosis in Fe_3O_4 NPs-treated human hepatoma SK-Hep-1 cells (**A**) and Hep3B cells (**B**).
Notes: Cells exposed to Fe_3O_4 NPs with different diameters for 24 hours were determined by flow cytometry. Cells incubated in medium only were used as control. Results correspond to mean ± SE of three independent experiments.
Abbreviations: NPs, nanoparticles; SE, standard error; FITC, fluorescein isothiocyanate; PE, phycoerythrin; PI, propidium iodide.

with SOD and CAT, as ROS scavengers,[20] during Fe_3O_4 NPs incubation. A typical result is illustrated in Figure 8A and B, where SOD plus CAT treatment effectively abolished the occurrence of cellular necrosis induced by 9 nm Fe_3O_4 NPs in both SK-Hep-1 and Hep3B cells. This implies that 9 nm Fe_3O_4 NPs potentiate cellular necrosis through promoting mitochondrial dysfunction and thus facilitating ROS accumulation.

Based on the abovementioned results, we know that 6 nm and 14 nm Fe_3O_4 NPs can also promote mitochondrial

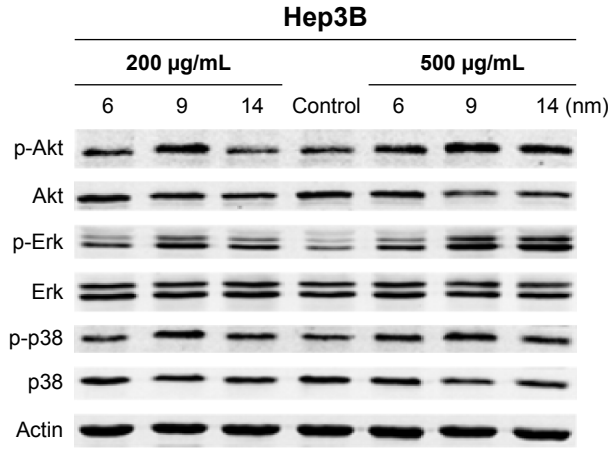

Figure 7 Fe_3O_4 NPs regulate the activities of Akt and MAPK in human hepatoma cells.
Notes: The expressions of Akt, Erk, and p38 were measured using Western blot in Hep3B cells exposed to Fe_3O_4 NPs with different diameters for 24 hours. Cells incubated in medium only were used as control.
Abbreviation: NPs, nanoparticles.

dysfunction and slight or moderate ROS production. However, the accumulation of ROS was proved to be non-related with cellular apoptosis or necrosis. To investigate whether Fe_3O_4 NPs effect on the cellular plasma membrane, the cellular membrane damage of Fe_3O_4 NPs was then evaluated using LDH leakage assay, which reports the loss of the integrity of plasma membrane. As shown in Figure 8C, following the exposure of SK-Hep-1 cells to 200 μg/mL Fe_3O_4 NPs for 24 hours, only the 14 nm Fe_3O_4 NPs produced significant LDH leakage compared to 6 nm Fe_3O_4 NPs and 9 nm Fe_3O_4 NPs. On the contrary, 500 μg/mL Fe_3O_4 NPs triggered an increase in LDH leakage in a diameter-dependent manner. In addition, the cytotoxicity of Fe_3O_4 NPs was also investigated by using Hep3B cells and similar behavior was further confirmed (Figure 8D). Notwithstanding, Hep3B cells appeared to be more sensitive compared to SK-Hep-1 cells, but 14 nm Fe_3O_4 NPs exerted strong cytotoxicity in LDH leakage for Hep3B cells without differences between doses of 200 μg/mL and 500 μg/mL. These findings demonstrate that 14 nm Fe_3O_4 NPs principally instigate to plasma membrane damage and cause LDH leakage.

It may seem contradictory that 14 nm Fe_3O_4 NPs treatment showed slighter mitochondrial dysfunction but stronger LDH leakage compared to 9 nm Fe_3O_4 NPs. To elucidate this difference, we also treated cells with SOD and CAT during Fe_3O_4 NPs incubation, and detected LDH leakage. As shown in Figure 8E and F, the increased LDH leakage induced by 6 nm and 9 nm Fe_3O_4 NPs was completely removed by SOD plus CAT pretreatment in both SK-Hep-1 and Hep3B cells. In contrast, SOD plus CAT pretreatment ameliorated the LDH leakage with 32.8% and 48.5% reduction in SK-Hep-1 cells treated with 14 nm Fe_3O_4 NPs at 200 μg/mL and 500 μg/mL, respectively, compared to cells without the pretreatment of SOD and CAT. These data further demonstrated that 9 nm Fe_3O_4 NPs primarily elicited mitochondrial dysfunction to trigger programmed necrosis predominantly through ROS signaling, while 14 nm Fe_3O_4 NPs exposure impaired the integrity of plasma membrane damage and promoted massive LDH leakage.

Discussion

The safety of Fe_3O_4 NPs is routinely estimated in vitro prior to applications in humans. Therefore, it is crucial to understand the mechanism of different diameter Fe_3O_4 NPs-induced cytotoxicity before we confidently use the results from laboratory to make deductions in human. The small size and the relatively large surface of NPs have been proved to increase the cytotoxicity when compared to particles with micrometer size. In addition, small particles are believed to interact more strongly with biological systems. However, the internal mechanism of this increased cytotoxicity is not yet well understood. The current study first disclosed that 6 nm Fe_3O_4 NPs exhibited negligible cytotoxicity and 9 nm Fe_3O_4 NPs increased cytotoxicity via cellular mitochondrial dysfunction and induced necrosis. But, 14 nm Fe_3O_4 NPs predominantly led to plasma membrane damage. Consistently, this cytotoxicity of Fe_3O_4 NPs was associated with their cellular uptake and intracellular ROS generation.

As inductively coupled plasma mass spectrometry has significant advantages in measuring the cellular uptake of NPs, it has been used as a regular method. Since partial Fe_3O_4 NPs still adhere to the cell surface after the uptake, the inductively coupled plasma mass spectrometry could not distinguish the Fe_3O_4 NPs between adhered to the cell surface and internalized into the cell; therefore, it easily causes measurement errors. However, flow cytometric light scattering assay can solve this problem. This is mainly because the internalized NPs will aggregate within intracellular vesicles if the NPs are internalized into cells, which can change the light scattering of flow cytometry. By means of this property, the intracellular NP concentration can be accurately measured. Therefore, in this study, the cellular uptake of Fe_3O_4 NPs was carried out using flow cytometric light scattering assay, which was consistent with the internalized distribution detected by TEM in Figure 3, which further indicates that flow cytometry was more suitable for measuring cellular uptake of Fe_3O_4 NPs.

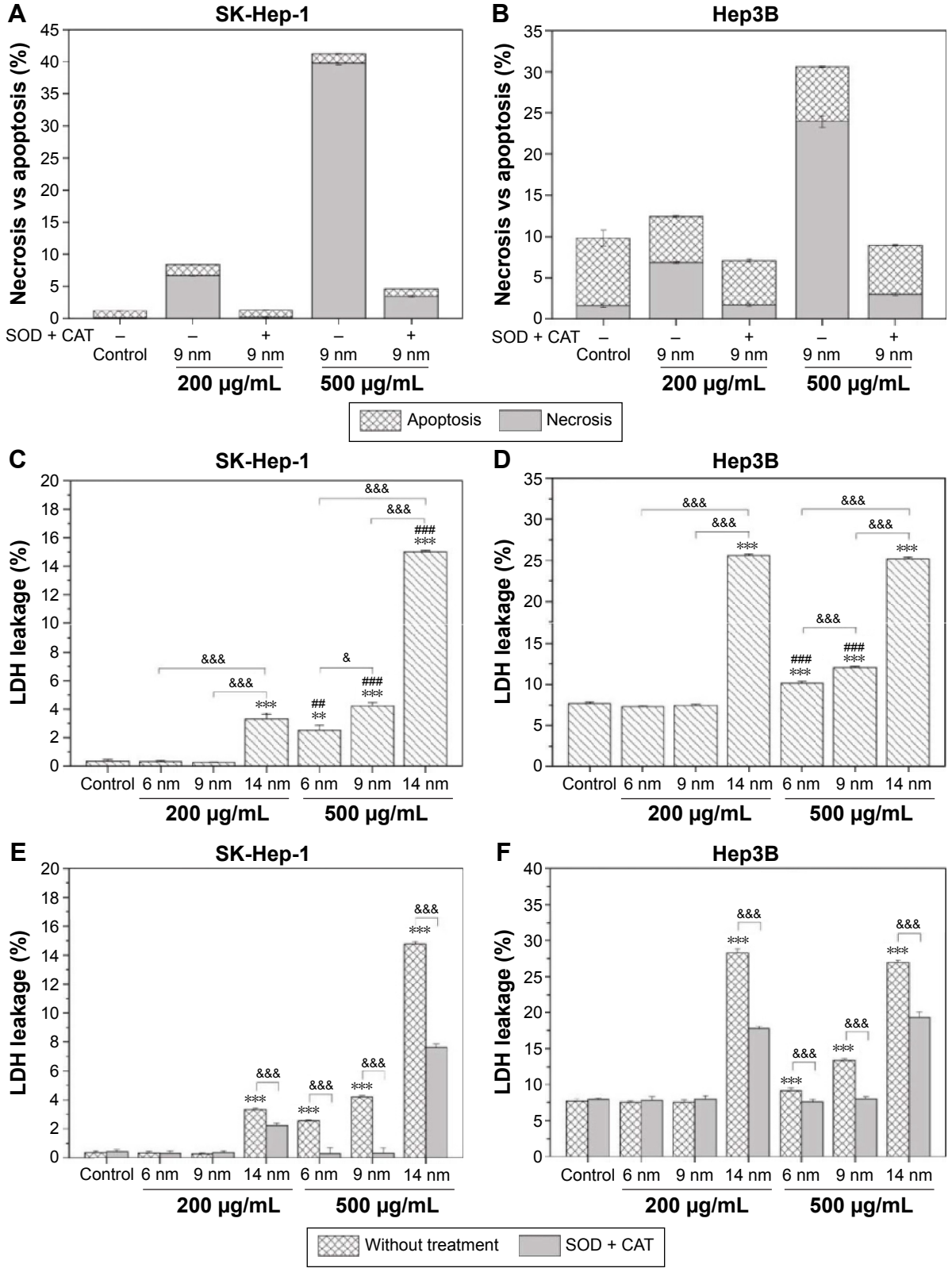

Figure 8 Influence of ROS scavenger on Fe_3O_4-induced necrosis and plasma membrane damage.

Notes: (**A** and **B**) ROS scavenger SOD and CAT suppressed Fe_3O_4 NPs-induced necrosis in human hepatoma SK-Hep-1 cells (**A**) and Hep3B cells (**B**). Cells exposed to Fe_3O_4 NPs with different diameters for 24 hours were determined by flow cytometry. Cells incubated in medium only were used as control. (**C**–**F**) Effect of Fe_3O_4 NPs on cellular membrane damage of human hepatoma SK-Hep-1 cells (**C** and **E**) and Hep3B cells (**D** and **F**). Cellular membrane damage of cells treated with different concentrations of Fe_3O_4 NPs with different diameters for 24 hours was measured by the LDH leakage assay. In some experiments, cells were incubated with SOD and CAT. Data are presented as mean ± SE of three independent experiments with triplicates in each case. $^{**}P<0.01$, $^{***}P<0.001$ compared to the control without Fe_3O_4 NPs treatment; $^{\#\#}P<0.01$, $^{\#\#\#}P<0.001$ compared to the corresponding Fe_3O_4 NPs treatment at 200 μg/mL; $^{\&}P<0.05$, $^{\&\&\&}P<0.001$ between the indicated groups.

Abbreviations: CAT, catalase; LDH, lactate dehydrogenase; NPs, nanoparticles; ROS, reactive oxygen species; SE, standard error; SOD, superoxide dismutase.

The cellular uptake amount of NPs and its internalization distribution in cells are key factors to induce cytotoxicity response. Mitochondria are vulnerable targets for cytotoxicity because of their crucial role in maintaining cellular function via aerobic adenosine triphosphate generation.[21] It was reported that the enhancement of intracellular uptake of protamine-modified maghemite NPs led to a significant impairment of cellular viability in human hepatoma cell line SMMC-7721.[22] Consistently, in this article, we report that 6 nm Fe_3O_4 NPs exhibited negligible effect on mitochondrial function, while 9 nm and 14 nm Fe_3O_4 NPs displayed mitochondrial dysfunction in a dose-dependent manner, where 9 nm Fe_3O_4 NPs played a more crucial role on mitochondrial dysfunction. These distinctive results may suggest a different mechanism for mitochondrial dysfunction induced by Fe_3O_4 NPs. Moreover, in response to Fe_3O_4 NPs, Hep3B cells displayed much more sensitivity than SK-Hep-1 cells. This slight difference probably resides in the intrinsic distinct characteristics of these two cell lines, in a different p53 status.[23] However, a recent study indicated that Fe_3O_4 NPs specifically impair liver mitochondrial coupling in middle-aged rats but not in young animals,[24] since SK-Hep-1 is a poor-differentiated hepatoma cell line, while Hep3B is a well-differentiated hepatoma cell line,[25] suggesting that these differences of Fe_3O_4 NPs for mitochondrial function inhibition are associated with the differentiation of cells.

Under physiological circumstances, ROS are the natural by-product of cellular metabolism process taking place in the mitochondria and have an important role in cellular homeostasis, which could be easily disturbed by outer environmental stress.[26] In addition, excess or exaggerated ROS production can cause mitochondrial dysfunction.[27] As expected, a significant increase in ROS was observed after exposure of cells to Fe_3O_4 NPs in a dose-dependent manner. Furthermore, at the same dosage, the intensity of Fe_3O_4 NPs induced intracellular ROS generation was on the tendency of 9 nm >14 nm >6 nm (Figure 5). These findings support the idea that ROS production is the main cause of mitochondrial dysfunction.

Overwhelming ROS generation represents the oxidative stress status, which overcomes the antioxidant protective ability of the cell and thus induces deleterious biological effects including mitochondrial dysfunction, DNA damage, apoptosis, and necrosis.[27] In addition, mitochondrial dysfunction can also lead to apoptosis or necrosis, which depends on the energy status of the cell.[28] As anticipated, our results showed that 9 nm Fe_3O_4 NPs predominantly contributed to cellular necrosis with negligible effect on apoptosis (Figure 6). Nevertheless, ROS scavengers SOD plus CAT treatment extensively suppressed the induction of cellular necrosis in the presence of 9 nm Fe_3O_4 NPs. Indeed, one vital function of mitochondria is to eliminate damaged cells by mitochondrial biogenesis in response to adenosine triphosphate depletion and oxidative stress.[29] More recently, Luo et al[30] demonstrated that superparamagnetic Fe_3O_4 NPs alone exhibited no toxicity in H9c2 cardiomyocyte cells but sensitized acrolein-induced cell dysfunction as reflected by ROS generation, mitochondrial dysfunction, and necrosis. These data suggested that the intracellular localization of 9 nm Fe_3O_4 NPs elicits ROS production to facilitate mitochondrial dysfunction, thus leading to cell necrosis.

Restoring or inducing cellular apoptosis and necrosis are potential strategies for cancer therapy. Several cellular and molecular biological characteristics could be found in the apoptotic and necrotic cells, including cell cycle assay, DNA damage, activation of the caspase cascade, and activation of MAPK pathway.[31] Furthermore, apoptosis and necrosis as well as many associated cellular mechanisms, including the regulation of PI3K/Akt/Bad pathway, induced by oxidative stress response have been observed.[32] In this study, we also confirmed that 9 nm Fe_3O_4 NPs-induced ROS generation would result in dramatically enhanced p-Akt, p-Erk, and p-p38. Previous study has showed that platinum NPs as anti-inflammatory agents significantly reduced the lipopolysaccharide-induced production of intracellular ROS and suppressed the phosphorylation of Erk and Akt.[33] Analogously, superparamagnetic Fe_3O_4 NPs have also been reported to sensitize acrolein-induced ROS generation for the activation of Erk.[30] Thus, these results in combination with our findings support the concept that the generation of ROS is required for Akt phosphorylation at Ser473[34] and Erk activation, which further stimulate cell necrosis.[35] In addition, p38 activation is widely believed to be pro-apoptotic in nature.[36] Overall, PI3K/Akt/Bad and MAPK pathways are involved in 9 nm Fe_3O_4 NPs-induced cell apoptosis and necrosis.

Previously, LDH leakage was termed as the secondary necrosis pathway in the apoptotic process and often used as a marker of necrosis, since apoptotic cell body at the late stage was subjected to cellular membrane collapse.[37] This is in contrast with our findings that 14 nm Fe_3O_4 NPs elicited strong LDH leakage but negligible effect on cell apoptosis and necrosis, and the LDH leakage induced by 14 nm Fe_3O_4 NPs could be partially ameliorated by the treatment of ROS scavengers. However, the TEM images (Figure 3) illustrated that after cellular uptake through phagocytosis, the intracellular accumulation of 9 nm Fe_3O_4 NPs presented

in the agglomerated state, which might excite more severe cell oxidative stress than 6 nm and 14 nm Fe_3O_4 NPs, and hence compromise mitochondrial dysfunction to elicit higher intracellular ROS levels and necrosis/apoptosis. Nonetheless, 6 nm and 14 nm Fe_3O_4 NPs dispersed in the cells, where 14 nm Fe_3O_4 NPs provoked autophagic vacuoles, which would switch into impairment of cytoskeleton and secondary necrosis, and then resulted in cell membrane rupture and allowed aggravated LDH release from the cells.

Conclusion

This study clearly elucidated the cellular uptake and internalization of small Fe_3O_4 NPs with different diameters and their mechanisms of toxicological hazards in SK-Hep-1 and Hep3B hepatoma cells, in which 6 nm Fe_3O_4 NPs exhibited negligible cytotoxicity and 9 nm Fe_3O_4 NPs increased cytotoxicity via cellular mitochondrial dysfunction, and hence induced necrosis that was mediated through mitochondria-dependent intracellular ROS generation, while 14 nm Fe_3O_4 NPs predominantly led to plasma membrane damage partially in a ROS generation-dependent manner. The study provides a foundation to incorporate in vivo toxicity data for quantitative risk assessment and could be extrapolated to other types of NPs and NPs-based drugs for safety evaluation in clinical application.

Acknowledgments

We gratefully acknowledge the financial support by the National Natural Science Foundation of China (Nos 31400719, 81472842, 81402548, and 81560495), the Experimental Animal Project from Science and Technology Commission of Shanghai (No 15140902700), the Scientific Research Innovation Program from the Shanghai Municipal Education Commission (14YZ029), Shanghai Municipal Commission of Health and Family Planning (No 20144Y0203), the Medical-Engineering Joint Funds from the Shanghai Jiao Tong University (No YG2011MS53), and the Fund of Shanghai Jiao Tong University School of Medicine (No 12XJ10079).

Disclosure

The authors report no conflicts of interest in this work.

References

1. Lewin M, Carlesso N, Tung CH, et al. Tat peptide-derivatized magnetic nanoparticles allow in vivo tracking and recovery of progenitor cells. *Nat Biotechnol*. 2000;18(4):410–414.
2. Pittet MJ, Swirski FK, Reynolds F, Josephson L, Weissleder R. Labeling of immune cells for in vivo imaging using magnetofluorescent nanoparticles. *Nat Protoc*. 2006;1(1):73–79.
3. Chalmers JJ, Xiong Y, Jin X, et al. Quantification of non-specific binding of magnetic micro- and nanoparticles using cell tracking velocimetry: implication for magnetic cell separation and detection. *Biotechnol Bioeng*. 2010;105(6):1078–1093.
4. Cai X, Cai X, Wang C, et al. Antitumor efficacy of DMSA modified Fe3O4 magnetic nanoparticles combined with arsenic trioxide and adriamycin in Raji cells. *J Biomed Nanotechnol*. 2014;10(2):251–261.
5. Chertok B, Moffat BA, David AE, et al. Iron oxide nanoparticles as a drug delivery vehicle for MRI monitored magnetic targeting of brain tumors. *Biomaterials*. 2008;29(4):487–496.
6. Ito A, Kuga Y, Honda H, et al. Magnetite nanoparticle-loaded anti-HER2 immunoliposomes for combination of antibody therapy with hyperthermia. *Cancer Lett*. 2004;212(2):167–175.
7. Ma N, Ma C, Li C, et al. Influence of nanoparticle shape, size, and surface functionalization on cellular uptake. *J Nanosci Nanotechnol*. 2013;13(10):6485–6498.
8. Ling D, Hyeon T. Chemical design of biocompatible iron oxide nanoparticles for medical applications. *Small*. 2013;9(9–10):1450–1466.
9. Alarifi S, Ali D, Alkahtani S, Alhader MS. Iron oxide nanoparticles induce oxidative stress, DNA damage, and caspase activation in the human breast cancer cell line. *Biol Trace Elem Res*. 2014;159(1–3):416–424.
10. Smith MJ, Brown JM, Zamboni WC, Walker NJ. From immunotoxicity to nanotherapy: the effects of nanomaterials on the immune system. *Toxicol Sci*. 2014;138(2):249–255.
11. Gupta AK, Gupta M. Synthesis and surface engineering of iron oxide nanoparticles for biomedical applications. *Biomaterials*. 2005;26(18):3995–4021.
12. Gaumet M, Vargas A, Gurny R, Delie F. Nanoparticles for drug delivery: the need for precision in reporting particle size parameters. *Eur J Pharm Biopharm*. 2008;69(1):1–9.
13. Mishra AR, Zheng J, Tang X, Goering PL. Silver nanoparticle-induced autophagic-lysosomal disruption and NLRP3-inflammasome activation in HepG2 cells is size-dependent. *Toxicol Sci*. 2016;150(2):473–487.
14. Kang JH, Toita R, Murata M. Liver cell-targeted delivery of therapeutic molecules. *Crit Rev Biotechnol*. 2016;36(1):132–143.
15. Adrian JE, Poelstra K, Scherphof GL, et al. Interaction of targeted liposomes with primary cultured hepatic stellate cells: involvement of multiple receptor systems. *J Hepatol*. 2006;44(3):560–567.
16. Giannitrapani L, Soresi M, Bondi ML, Montalto G, Cervello M. Nanotechnology applications for the therapy of liver fibrosis. *World J Gastroenterol*. 2014;20(23):7242–7251.
17. Dong L, Zuo L, Xia S, et al. Reduction of liver tumor necrosis factor-alpha expression by targeting delivery of antisense oligonucleotides into Kupffer cells protects rats from fulminant hepatitis. *J Gene Med*. 2009;11(3):229–239.
18. Cai W, Wan J. Facile synthesis of superparamagnetic magnetite nanoparticles in liquid polyols. *J Colloid Interface Sci*. 2007;305(2):366–370.
19. Liu P, Sun Y, Wang Q, Sun Y, Li H, Duan Y. Intracellular trafficking and cellular uptake mechanism of mPEG-PLGA-PLL and mPEG-PLGA-PLL-Gal nanoparticles for targeted delivery to hepatomas. *Biomaterials*. 2014;35(2):760–770.
20. Xie YX, Tu WZ, Zhang JH, et al. SirT1 knockdown potentiates radiation-induced bystander effect through promoting c-Myc activity and thus facilitating ROS accumulation. *Mutat Res*. 2015;772:23–29.
21. Wang P, Liu J, Li Y, et al. Peroxisome proliferator-activated receptor {delta} is an essential transcriptional regulator for mitochondrial protection and biogenesis in adult heart. *Circ Res*. 2010;106(5):911–919.
22. Xia JG, Zhang S, Zhang Y, Ma M, Gu N. Maghemite nanoparticles and their protamine derivatives: cellular internalization and effects on cell-cycle progress. *J Nanosci Nanotechnol*. 2009;9(2):1025–1028.
23. Kuo TC, Chang PY, Huang SF, Chou CK, Chao CC. Knockdown of HURP inhibits the proliferation of hepatocellular carcinoma cells via downregulation of gankyrin and accumulation of p53. *Biochem Pharmacol*. 2012;83(6):758–768.

24. Baratli Y, Charles AL, Wolff V, et al. Age modulates Fe3O4 nanoparticles liver toxicity: dose-dependent decrease in mitochondrial respiratory chain complexes activities and coupling in middle-aged as compared to young rats. *Biomed Res Int*. 2014;2014:474081.
25. Wu TT, Hsieh YH, Hsieh YS, Liu JY. Reduction of PKC alpha decreases cell proliferation, migration, and invasion of human malignant hepatocellular carcinoma. *J Cell Biochem*. 2008;103(1):9–20.
26. Sabharwal SS, Schumacker PT. Mitochondrial ROS in cancer: initiators, amplifiers or an Achilles' heel? *Nat Rev Cancer*. 2014;14(11):709–721.
27. Marchi S, Giorgi C, Suski JM, et al. Mitochondria-ROS crosstalk in the control of cell death and aging. *J Signal Transduct*. 2012;2012:329635.
28. Smith MA, Schnellmann RG. Calpains, mitochondria, and apoptosis. *Cardiovasc Res*. 2012;96(1):32–37.
29. Bellanti F, Romano AD, Giudetti AM, et al. Many faces of mitochondrial uncoupling during age: damage or defense? *J Gerontol A Biol Sci Med Sci*. 2013;68(8):892–902.
30. Luo C, Li Y, Yang L, Wang X, Long J, Liu J. Superparamagnetic iron oxide nanoparticles exacerbate the risks of reactive oxygen species-mediated external stresses. *Arch Toxicol*. 2015;89(3):357–369.
31. Owuor ED, Kong AN. Antioxidants and oxidants regulated signal transduction pathways. *Biochem Pharmacol*. 2002;64(5–6):765–770.
32. Fang L, Chen B, Liu S, et al. Synergistic effect of a combination of nanoparticulate Fe3O4 and gambogic acid on phosphatidylinositol 3-kinase/Akt/Bad pathway of LOVO cells. *Int J Nanomedicine*. 2012;7:4109–4118.
33. Rehman MU, Yoshihisa Y, Miyamoto Y, Shimizu T. The anti-inflammatory effects of platinum nanoparticles on the lipopolysaccharide-induced inflammatory response in RAW 264.7 macrophages. *Inflamm Res*. 2012;61(11):1177–1185.
34. Huang C, Li J, Ding M, et al. UV Induces phosphorylation of protein kinase B (Akt) at Ser-473 and Thr-308 in mouse epidermal Cl 41 cells through hydrogen peroxide. *J Biol Chem*. 2001;276(43):40234–40240.
35. Chou WW, Chen KC, Wang YS, Wang JY, Liang CL, Juo SH. The role of SIRT1/AKT/ERK pathway in ultraviolet B induced damage on human retinal pigment epithelial cells. *Toxicol In Vitro*. 2013;27(6):1728–1736.
36. Tewari R, Sharma V, Koul N, Sen E. Involvement of miltefosine-mediated ERK activation in glioma cell apoptosis through Fas regulation. *J Neurochem*. 2008;107(3):616–627.
37. Majno G, Joris I. Apoptosis, oncosis, and necrosis. An overview of cell death. *Am J Pathol*. 1995;146(1):3–15.